Solar Energy 135 (2016) 22–28

Contents lists available at ScienceDirect

Solar Energy

journal homepage: www.elsevier.com/locate/solener

Enhanced open-circuit voltage of dye-sensitized solar cells using Bi-doped TiO_2 nanofibers as working electrode and scattering layer

Ming-Chung Wu [a,b,c,*], Wei-Cheng Chen [a], Ting-Han Lin [a], Kai-Chi Hsiao [a], Kun-Mu Lee [d,e,*], Chun-Guey Wu [e,*]

[a] Department of Chemical and Materials Engineering, College of Engineering, Chang Gung University, Taoyuan 33302, Taiwan
[b] Center for Reliability Sciences & Technologies, Chang Gung University, Taoyuan 33302, Taiwan
[c] Division of Neonatology, Department of Pediatrics, Chang Gung Memorial Hospital, Taoyuan 33305, Taiwan
[d] Department of Chemical and Materials Engineering, National Central University, Taoyuan 32001, Taiwan
[e] Research Center for New Generation Photonics, National Central University, Taoyuan 32001, Taiwan

ARTICLE INFO

Article history:
Received 10 November 2015
Received in revised form 26 April 2016
Accepted 15 May 2016
Available online 30 May 2016

Keywords:
Dye-sensitized solar cells
Bi-doped TiO_2
Nanofiber
Hydrothermal synthesis

ABSTRACT

Doping metal-ion into TiO_2 materials is an effective method for enhancing the performance of dye-sensitized solar cells (DSSCs). In order to develop materials that are easy to produce even in industrial quantities, we established a facile method by hydrothermal synthesis and subsequent heat treatment to prepare bismuth doped titanium dioxide nanofibers (Bi-doped TiO_2 NFs). At first, we adopt Bi-doped TiO_2 NFs as the working electrode to further study in DSSCs. Serving as working electrode, Bi-doped TiO_2 NFs can remarkably improve open-circuit voltage (V_{OC}). The V_{OC} was significantly enhanced from 0.633 V to 0.800 V compared with pristine TiO_2 does. However, this leads to a smaller J_{SC} and a poorer overall performance for such devices. In order to improve the performance of DSSCs, we adopt Bi-doped TiO_2 NFs as the scattering layer of DSSCs, and various thicknesses of meso-TiO_2 nanoparticles (meso-TiO_2 NPs) were used as working electrode to increase the short-circuit current (J_{SC}). The incorporated Bi-doped TiO_2 NFs can help the electron transport and may reduce the possibility for electron–hole recombination. After optimizing the device's parameter, the overall performance of the meso-TiO_2 NPs/Bi-doped TiO_2 NFs devices was dominated by J_{SC} until a maximum efficiency was attained with a meso-TiO_2 NPs thickness of 12 μm. Such optimized DSSCs exhibited high open circuit voltage of 0.787 V, high fill factor of 78.2%, and high power conversion efficiency of 8.89%.

1. Introduction

Dye-sensitized solar cells attract a lot of interests due to its low cost, colorful, flexible, easy production, and acceptable efficiency when compared to conventional silicon solar cells (O'Regan and Gratzel, 1991; Yella et al., 2011; Chen et al., 2009; Chiappara et al., 2016). One of the key factors to achieve high performance DSSCs is the choice of the mesoporous TiO_2 working electrode and light scattering layer. The concept is to include a light scattering layer such that the lower photon conversion due to thin mesoporous TiO_2 layer could be compensated (Hore et al., 2006). TiO_2 and its derivatives are in the mainstream of energy and environmental science studies because of their availability, low cost, tuneable electron transport behavior, high photocatalytic activity, and thermal and chemical stability (Horváth et al., 2007; Konstantinou and Albanis, 2004; Ong et al., 2014; Sarkar et al., 2012; Wu et al., 2012). TiO_2 and its derivatives can be applied in a number of different fields such as air purification, wastewater treatment, photocatalytic hydrogen generation, antimicrobial coatings, photovoltaic, among many others (Kudo and Miseki, 2009; Kudo et al., 2004; Zhang et al., 2010). In a number of practical applications, nanofibers can perform much better than the corresponding nanoparticles. It is vital to have a percolated electrical network of the particles in electrical devices employing nanoparticles, which is much easier to achieve with elongated 1-dimensional particles than with ordinary 0-dimensional nanoparticles (Lin et al., 2009).

Many researchers used diameter of 300–400 nm sub-micro TiO_2 particle and controlled thickness of 3–4 μm as the scattering layer of TiO_2. Jun et. al. used open-ended TiO_2 nanotube arrays as

* Corresponding authors at: Department of Chemical and Materials Engineering, College of Engineering, Chang Gung University, Taoyuan 33302, Taiwan (M.-C. Wu). Department of Chemical and Materials Engineering, National Central University, Taoyuan 32001, Taiwan (K.-M. Lee). Research Center for New Generation Photonics, National Central University, Taoyuan 32001, Taiwan (C.-G. Wu).

E-mail addresses: mingchungwu@mail.cgu.edu.tw (M.-C. Wu), kmlee@ncu.edu.tw (K.-M. Lee), t610002@cc.ncu.edu.tw (C.-G. Wu).

http://dx.doi.org/10.1016/j.solener.2016.05.021
0038-092X/

scattering layer to enhance the power conversion efficiency (PCE) of DSSCs. With the TiO_2 scattering layer, the PCE was increased from 5.92% to 6.53%, which is attributed to improve the light harvesting of longer wavelength (600–800 nm) (Rho et al., 2014). Chou et. al. reported that the a DSSCs achieved a PCE of 7.02%, with a hybrid TiO_2 electrode consisted of 50% TiO_2 nanoparticles and 50% sub-micro TiO_2 particles, substantially exceeds that of only with a TiO_2 nanoparticles electrode (PCE ~ 5.16%) due to the effect of the light scattering in the DSSCs (Chou et al., 2012). Moreover, the synthesized rice-like brookite TiO_2 submicrometer particles and commercial nanosized anatase TiO_2 paste were also used to fabricate the bilayer TiO_2 film-based DSSCs. Their results show that the rice-like brookite TiO_2 particles can noticeably improve the performances of the nanosized anatase TiO_2 film-based solar cell when applied as scattering overlayer on nanosized anatase TiO_2 (Xu et al., 2014).

Metal-doped TiO_2 materials used as working electrodes and light scattering layers are studied in recent years for enhancing performance of DSSCs (Lü et al., 2010; Ghanbari Niaki et al., 2014; Nikolay et al., 2011; Park and Han, 2014; Moghaddam et al., 2016). In order to improve DSSCs performance, Er^{3+} and Yb^{3+} co-doped $TiO_{2-x}F_x$ was fabricated via hydrothermal method and was subsequently calcined in atmosphere. The result exhibited the lower band gap which contributed to a faster electrons injection and decreased the radiative recombination process of photogenerated electrons and holes in TiO_2 (Yu et al., 2013). Lü et. al. reported an overall 7.8% PCE obtained for a Nb-doped TiO_2, which had a large PCE improvement relative to that of undoped TiO_2 electrode for DSSCs. The improvement was ascribed to the enhanced electron-injection and electron-transfer efficiency caused by the increased powder conductivity, and the mechanism was verified by powder-resistance and EIS analyses (Lü et al., 2010). Nikolay et al. had found that the photovoltaic parameters of DSSCs based on Nb-doped TiO_2 can be sensitized with dyes that are closely related to the electronic structure of Nb-doped TiO_2 electrode. The changes of J_{SC} and V_{OC} of DSSCs were explained in relation to the electronic structure of Nb-doped TiO_2, and the highest PCE of 8.0% was achieved (Nikolay et al., 2011).

Dimensionality of TiO_2 nanomaterials is a crucial factor of carrier transportation. The morphology of nanofiber is confirmed to enhance transportation of carriers, and it could lead to efficient charge separation through interparticle charge transfer along the nanofiber framework (Li et al., 2011). The remarkable electron diffusion length on dye-sensitized solar cells based on TiO_2 nanofiber photoanodes played an important role in carrier transportation, so we can obtain high photocurrent and high PCE by utilizing thick TiO_2 nanofiber photoanodes (Ding et al., 2013).

In this work, we successfully synthesized Bi-doped TiO_2 nanofibers (Bi-doped TiO_2 NFs) by hydrothermal method, and Bi-doped TiO_2 NFs was adopted as the work electrode and the scattering layer for DSSCs. The optimal photovoltaic device exhibited a high open-circuit voltage, a high fill factor, and a high PCE of 8.89%. To our best knowledge, this is the first report to use Bi-doped TiO_2 NFs as the working electrode and the scattering layer TiO_2 electrode for DSSCs and get a high PCE of more than 8% (under 100 mW/cm^2, AM 1.5G).

2. Experimental details

Bismuth doped sodium hydrogen titanate nanofibers were prepared by suspending 1000.0 mg TiO_2 anatase powder (Acros Organics, 98%) and 61.3 mg of bismuth nitrate (Acros Organics, 99.999%) in 25.0 mL 10.0 M NaOH aqueous solution, followed by a treatment in a Teflon-lined stainless steel autoclave at 150 °C for 24 h. The product was washed with deionized water, filtered and dried in air at 70 °C, then washed with 0.1 M HCl to exchange Na^+-ion for protons. The product was washed with deionized water, filtered and dried in air at 70 °C again. Then, the products doped with various bismuth concentrations were calcined at different temperatures with a heating rate of 5 °C/min for various calcination times.

The nanocrystalline TiO_2 was dispersed in α-terpineol with ethyl cellulose as binder to form a TiO_2 paste. The mesoporous TiO_2 (meso-TiO_2) films were prepared on F-doped SnO_2 transparent conducting oxide (FTO) glass using the screen printing method. The thickness of the TiO_2 film was controlled from 3 μm to 15 μm and the area of active TiO_2 electrode was 0.16 cm^2, and the thickness of meso-TiO_2 films were measured by Dektak 150 Surface Profiler. The film was sintered at 500 °C for 1 h in an open atmosphere and cooled at room temperature. Then, it was immersed in a solution of 0.5 mM N719 (uniregion bio. Tec.) in a mixture of solvents containing acetonitrile and tert-butanol (v/v = 1/1) at 40 °C for 12 h. The dye-loaded TiO_2 film was then rinsed with acetonitrile to remove the excess dye. The reduced Pt nanoparticles from H_2PtCl_6 by $NaBH_4$ solution on FTO glass was used as the counter electrodes of the DSSCs. The electrolyte used for measuring *J–V* curve of the DSSC consisted of 0.80 M PMII, 0.10 M LiI, 0.04 M I_2 and 0.50 M TBP in acetonitrile. The dye-loaded photoelectrode and the counter electrode were separated by a 60 μm thick hot-melt spacer (Surlyn, Dupont).

The crystalline structures of various thermally treated Bi-doped TiO_2 catalysts were measured by X-ray diffractometer (XRD, Bruker, D2 phaser with Xflash 430, Germany), and UV–vis absorption spectra were measured by absorption spectrophotometer (JASCO Analytical Instruments, V-630, Japan) in the 300–900 nm wavelength range. The specific surface area of the used nanofibers were measured by BET (Micromeritics ASAP2000). The microstructures of diameter/structure of Bi-doped TiO_2 NFs were observed by Spherical-aberration Corrected Field Emission Transmission Electron Microscope (JEOL, JEM-ARM200FTH, Japan). AM 1.5G solar simulator (Yamashita Denso, YSS-100A) was used as the irradiation source for the current density–voltage (*J–V*) measurement. The intensity of the simulated sunlight was calibrated to be 100 mW/cm^2 by a silicon photodiode. Related data were collected by an electrochemical analyzer (Autolab, PGSTAT30) at 25 °C.

3. Results and discussion

In order to discover the bismuth doping effects, XRD patterns of pristine TiO_2 NFs and 1.00 mol% Bi-TiO_2 NFs calcined at 600 °C for 12 h are shown in Fig. 1. Moreover, the XRD patterns of the hydrogen sodium titanate (HST) nanofibers and 1.00 mol% Bi-doped HST

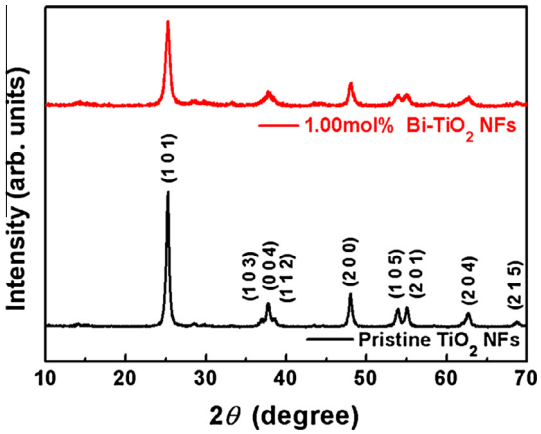

Fig. 1. XRD patterns of pristine TiO_2 NFs and 1.00 mol% Bi-doped TiO_2 NFs.

nanofibers calcined at various temperatures for 12 h were measured to understand the correlation between crystalline structure and calcination temperature (Fig. S1). Bi-TiO_2 NFs still exhibits TiO_2 anatase phase when the bismuth doping concentration is occurred. All the peaks can be indexed as the body-centered tetragonal lattice structure [JCPDS No. 89-4921] of anatase phase, with lattice constants $a = b = 3.78$ Å and $c = 9.50$ Å. However, the intensity of diffraction at 2θ of 25.3° decreased as the bismuth doping occurred, indicating the ordering of the lattice was destroyed when bismuth ions had entered into TiO_2 anatase structure. The specific surface area is an important information for preparing high-performance photocatalyst, because it is related to the surface reaction rate, resulting in the proportional relation between specific surface area and photocatalytic activity. The specific surface areas of pristine TiO_2 NFs and Bi-TiO_2 NFs are ~163.088 m^2/g and ~178.803 m^2/g, respectively, and the differences of their specific surface areas are less than 10%.

In order to find out the correlation between the absorption behavior and bismuth doping, the normalized absorption spectra of pristine TiO_2 NFs and 1.00 mol% Bi-doped TiO_2 NFs are measured as shown in Fig. 2. We can observe that when bismuth ion was doped into TiO_2 anatase structure, the reflection spectrum clearly extends into the visible region, which means that the band gap of 1.00 mol% Bi-doped TiO_2 NFs decreased as Bi doping.

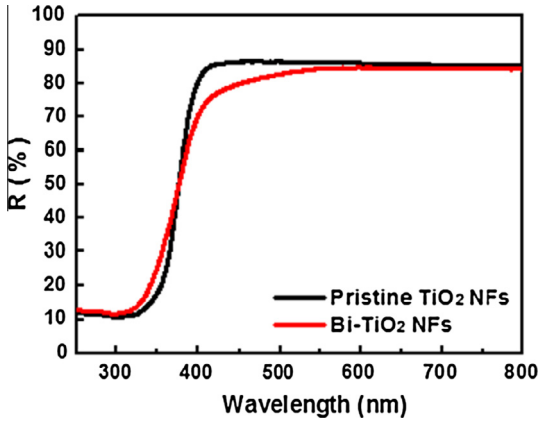

Fig. 2. UV–vis reflection spectra of pristine TiO_2 NFs and 1.00 mol% Bi-doped TiO_2 NFs.

Microstructures of pristine TiO_2 NFs and 1.00 mol% Bi-doped TiO_2 NFs are shown in Fig. 3. The pristine TiO_2 NFs had a length of up to 10 μm and a diameter of ~100 nm as shown in Fig. 3a. For 1.00 mol% Bi-doped TiO_2, it showed a length of 5 μm and a similar diameter of ~100 nm as shown in Fig. 3d. The high-magnification lattice images of pristine TiO_2 NFs and 1.00 mol% Bi-doped TiO_2 NFs are shown in Fig. 3b and e, respectively. The corresponding fast Fourier transformed patterns of these specimen are used to check (1 0 1) crystal plane, and the increased d spacing for the (1 0 1) crystal plane is observed for 1.00 mol% Bi-doped TiO_2. The (1 0 1) spacing changed from 3.46 Å to 3.53 Å, when bismuth ion was doped into pristine TiO_2 NFs (Wu et al., 2014).

In order to design the high power conversion efficiency device, we need to understand the mechanism of DSSCs firstly. The mechanism of DSSCs can be divided into a few parts (Fig. 4). In the beginning, the incident light passes through the FTO substrate, and the photons are absorbed by the dyes adsorbed on the TiO_2 working electrode. Then, the excited electrons move from HOMO to LUMO of dye. After the electrons are excited, the pathway of excited electrons is transferred from LUMO of dye to the conduction band of working electrode and then to FTO layer. The electrons migrate from FTO to the counter electrode, which is formed by Pt, and react with electrolyte system. However, when the excited electrons of LUMO transfer to conduction band of working electrode, there are three negative reactions, which might be happening. First one, the excited electrons might return to HOMO and recombination happens during the fact that incident light excite the electrons of dye. Second one, the excited electrons transfer from LUMO of dye to the conduction band of working electrode then return to HOMO of dye. Third one, the excited electrons at conduction band of working electrode might redox with electrolyte. In order to prevent these negative reactions and enhance the power conversion efficiency, 1.00 mol% Bi-doped TiO_2 is adopted in this study. In Fig. 5a, the illustration shows four different DSSC structures, including the structures having 3 μm-thick pristine TiO_2 NFs **(Device I)** and 3 μm-thick 1.00 mol% Bi-doped TiO_2 NFs **(Device II)** as working electrode, and the DSSC structures having 3 μm thick

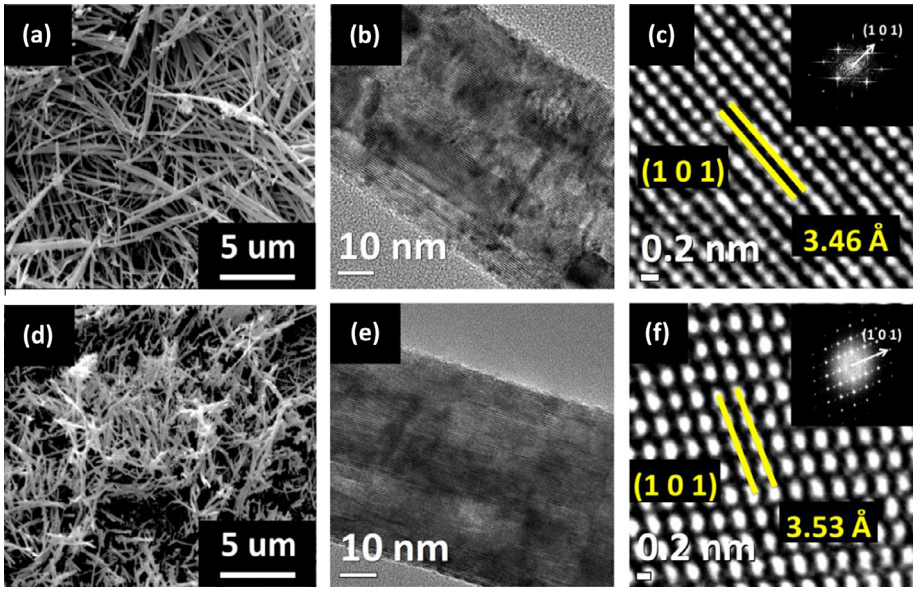

Fig. 3. (a and d) SEM micrographs, (b and e) TEM micrographs, and (c and f) high-magnification TEM micrographs of the lattice of pristine TiO_2 NFs and 1.00 mol% Bi-doped TiO_2 NFs.

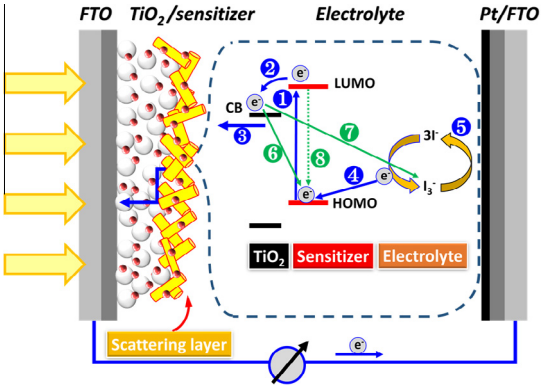

Fig. 4. The mechanism of dye sensitized solar cell. The electron transportation pathways of TiO_2, sensitizer, and electrolyte were proposed. (1) photoexitation; (2) electron injection; (3) electron transport (to FTO through mesoporous TiO_2 film); (4) regeneration of the oxidized dye; (5) reduction of electrolyte redox species; (6) reduction of oxidized dye by electron in E_{cb} of TiO_2; (7) interception of electron in E_{cb} of TiO_2 by electrolyte species, and (8) radiative or non-radiative decay of photoexcited electron.

meso-TiO_2 NPs layer as working electrode, and each with a 3 μm-thick pristine TiO_2 NFs **(Device III)** and Bi-doped TiO_2 NFs **(Device IV)** as the scattering layer. Shown in Table 1, the variation of V_{OC} is remarkable in that V_{OC} was significantly enhanced from 0.630 V **(Device I)** to 0.800 V **(Device II)** (Fig. 5b), and from 0.663 V **(Device III)** to 0.808 V **(Device IV)** (Fig. 5c). Bi-doped TiO_2 NFs exhibited higher value of the V_{OC} compared with pristine TiO_2 NFs, but Bi-doped TiO_2 NFs showed the lower value of J_{SC} than it of pristine

Table 1
Device performances of DSSCs based on different working electrodes and with/without scattering layers. (The thickness of meso-TiO_2 layer of device III and device IV are only ~3 μm).

Structure	V_{OC} (V)	J_{SC} (mA/cm$_2$)	FF (%)	PCE (%)
Device I	0.630 ± 0.001	0.54 ± 0.02	58.2 ± 0.21	0.20 ± 0.01
Device II	0.800 ± 0.001	0.41 ± 0.01	60.5 ± 0.23	0.20 ± 0.01
Device III	0.663 ± 0.007	5.33 ± 0.15	61.8 ± 1.24	2.18 ± 0.03
Device IV	0.808 ± 0.008	5.75 ± 0.27	76.9 ± 1.45	3.57 ± 0.06

TiO_2 NFs. However, the TiO_2 NFs showed lower J_{SC} than TiO_2 nanoparticle indicated that titanium dioxide nanofiber shows poor adsorption ability of dye (N719) because of its minor specific surface area. In order to increase the adsorption of dye on TiO_2 electrode, the meso-TiO_2 NPs layers were both applied in **Device III** and **Device IV**. After inserted the meso-TiO_2 NPs layer into DSSCs, the J_{SC} is significantly improved due to the higher surface area and extra amount dye adsorption. The enhanced J_{SC} indicates that the Bi-doped TiO_2 layer can help carrier transport and can reduce charge recombination.

In this study, we can observe an enhanced open circuit voltage, when the DSSC incorporated with Bi-doped TiO_2 NFs. Fig. 6 shows the energy level diagram of present DSSCs incorporated Bi-doped TiO_2 NFs. An energy barrier would exist at the interface of two materials, meso-TiO_2 NPs layer and Bi-doped TiO_2 NFs layer. The electronic charge generation is caused by light irradiation from the FTO substrate side. The meso-TiO_2 NPs layer and Bi-doped TiO_2 NFs layer received the electron from the dye-N719. The incorporated Bi-doped TiO_2 NFs layer can increase the light scattering and the Fermi energy of TiO_2 electrode, and can reduce the

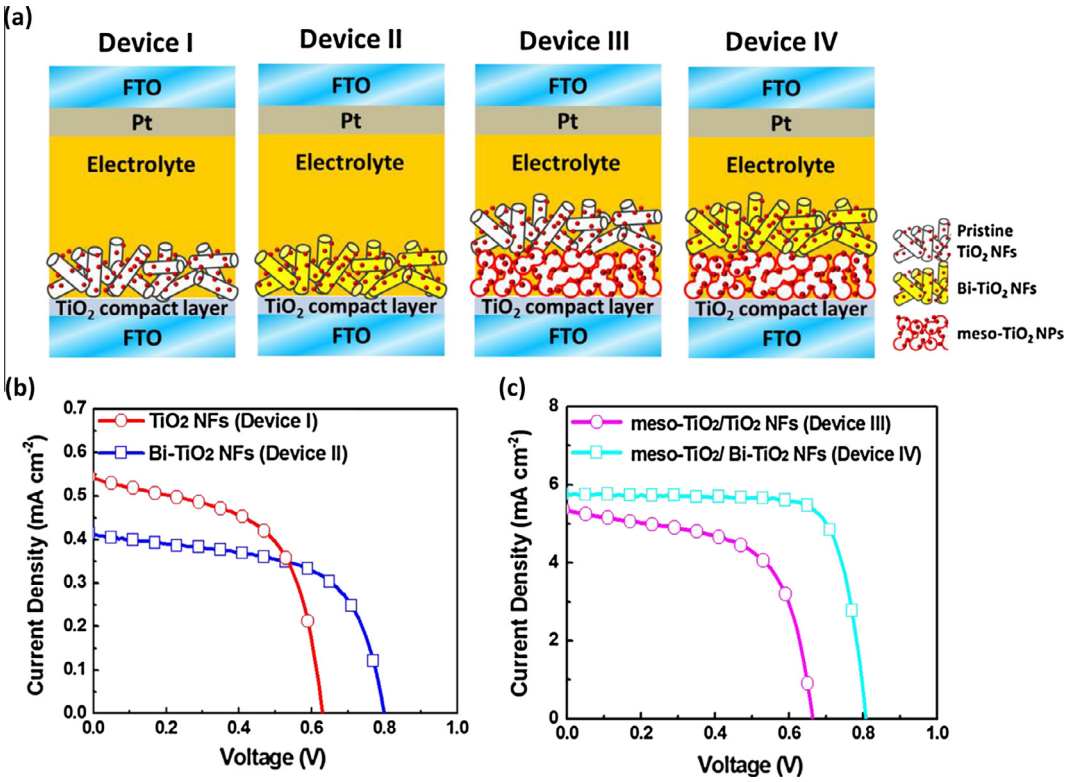

Fig. 5. (a) The schematic structures of various DSSCs in our study. The two left-side DSSCs structures are fabricated with pristine TiO_2 NFs (**Device I**) and Bi-doped TiO_2 NFs (**Device II**) as working electrode, respectively. The two right-side DSSCs structures having 3 μm thick meso-TiO_2 NPs as working electrode, and each with a 3 μm-thick pristine TiO_2 NFs (**Device III**) and Bi-doped TiO_2 NFs as the scattering layer (**Device IV**), respectively. (b) Photocurrent–voltage curves of the DSSCs with pristine TiO_2 NFs (red line) or Bi-doped TiO_2 NFs as working electrode (blue line). (c) Photocurrent–voltage curves of the DSSCs with pristine TiO_2 NFs (magenta line) and Bi-doped TiO_2 NFs as the scattering layer (cyan line), and each with a 3 μm thick meso-TiO_2 NPs as working electrode. (For interpretation of the references to colour in this figure legend, the reader is referred to the web version of this article.)

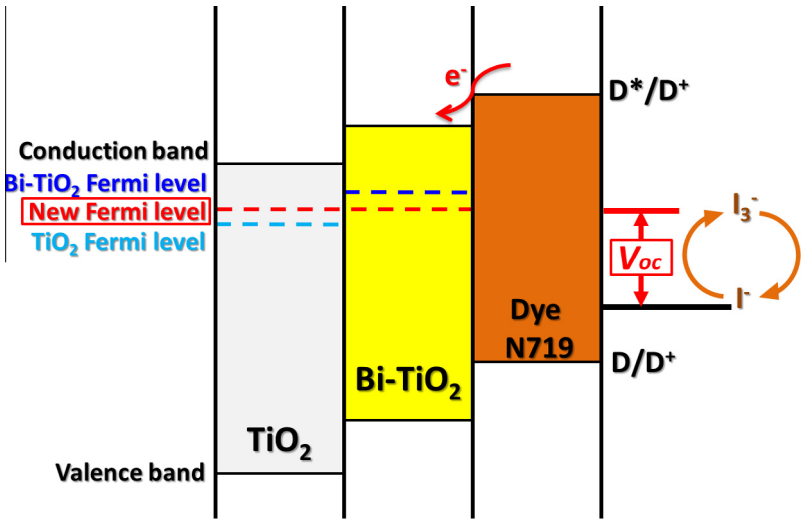

Fig. 6. Energy level diagram of the DSSCs with Bi-doped TiO_2 NFs as the scattering layer and with a meso-TiO_2 NPs as working electrode.

possibility for electron–hole recombination. In addition, we observed the open-circuit voltage increased from 0.663 V **(Device III)** to 0.808 V **(Device IV)** from Table 1. The existence of incorporated Bi-doped TiO_2 NFs layer, which possesses a higher conduction band minimum than meso-TiO_2 NPs layer, led to the Fermi level of working electrode (Bi-doped TiO_2 NFs/meso-TiO_2 NPs) variation and raised V_{OC}.

According to the marked performance of meso-TiO_2 NPs/Bi-doped TiO_2 NFs at a thin-film condition, we further tested the effect of film thickness of meso-TiO_2 on device performance with 3 μm Bi-doped TiO_2 NFs as light scattering layer. The thickness of the meso-TiO_2 NPs film was readily controllable across a broad range from 0 to 15 μm, and a thick meso-TiO_2 NPs film tended to crack when thickness is larger than 15 μm. Table 2 shows DSSCs device performance with Bi-doped TiO_2 NFs as the light scattering layer and various thickness of meso-TiO_2 NPs as working electrodes. The thickness of the Bi-doped TiO_2 NFs was fixed at ~3 μm. Fig. 7(a) shows the illustration of DSSCs structure with Bi-doped TiO_2 NFs as the scattering layer and the different thicknesses of meso-TiO_2 NPs as working electrode. The *J–V* curves obtained for the meso-TiO_2 NPs/Bi-doped TiO_2 NFs system are shown in Fig. 7(b).

Fig. 8a–d show the parameters, i.e. V_{OC}, J_{SC}, FF and PCE, as a function of the thickness of meso-TiO_2 NPs, respectively. The V_{OC} value of only Bi-doped TiO_2 NFs film is higher than that of meso-TiO_2 NPs/Bi-doped TiO_2 NFs, because it has a higher conduction band minimum than meso-TiO_2 NPs layer, led to the Fermi level of working electrode variation and raised V_{OC}. J_{SC} increased with larger amounts of dye loading on TiO_2 electrode as the thickness of meso-TiO_2 NFs increased. When the total thickness of meso-TiO_2 NPs layer is achieved ~12 μm, the DSSCs exhibits the maximum J_{SC} value of 14–15 mA/cm^2. The FF value shows no correlation with the thickness of meso-TiO_2 NFs, but the average value of meso-TiO_2 NPs/Bi-doped TiO_2 NFs is higher than that of only Bi-doped TiO_2 NFs film, which might indicate the advantage of meso-TiO_2 NPs/Bi-doped TiO_2 NFs film with better conductivity than that of only Bi-doped TiO_2 NFs film. The increased thickness of meso-TiO_2 NPs shows an increase in the short-circuit current owing to the fact that additional amount of dye-N719 was adsorbed by

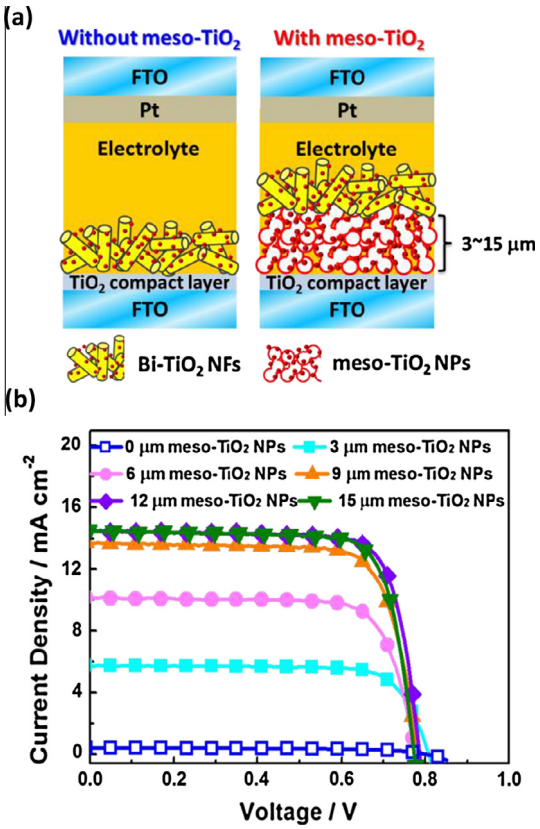

Fig. 7. (a) The schematic structures of DSSCs with/without the working electrode of meso-TiO_2 NPs layer, and each with a 3 μm-thick Bi-doped TiO_2 NFs as the scattering layer. (b) Photocurrent–voltage curves of DSSCs structure with different thickness of meso-TiO_2 NPs as working electrode, and each with a 3 μm-thick Bi-doped TiO_2 NFs as the scattering layer.

Table 2
Device performance of DSSCs with 3 μm Bi-doped TiO_2 NFs as the scattering layer and different thicknesses of meso-TiO_2 NPs films as working electrodes. Each DSSC performance is checked by more than three repetitions.

Thickness of meso-TiO_2 NPs film (μm)	V_{OC} (V)	J_{SC} (mA/cm$_2$)	FF (%)	PCE (%)
0	0.850 ± 0.001	0.41 ± 0.01	60.5 ± 0.20	0.21 ± 0.01
3	0.808 ± 0.008	5.75 ± 0.27	76.9 ± 1.45	3.57 ± 0.06
6	0.777 ± 0.002	10.11 ± 0.04	76.3 ± 0.15	5.99 ± 0.02
9	0.783 ± 0.012	13.62 ± 0.33	76.3 ± 0.43	8.14 ± 0.24
12	0.787 ± 0.006	14.45 ± 0.21	78.2 ± 2.52	8.89 ± 0.24
15	0.772 ± 0.021	14.51 ± 0.48	77.7 ± 0.51	8.70 ± 0.05

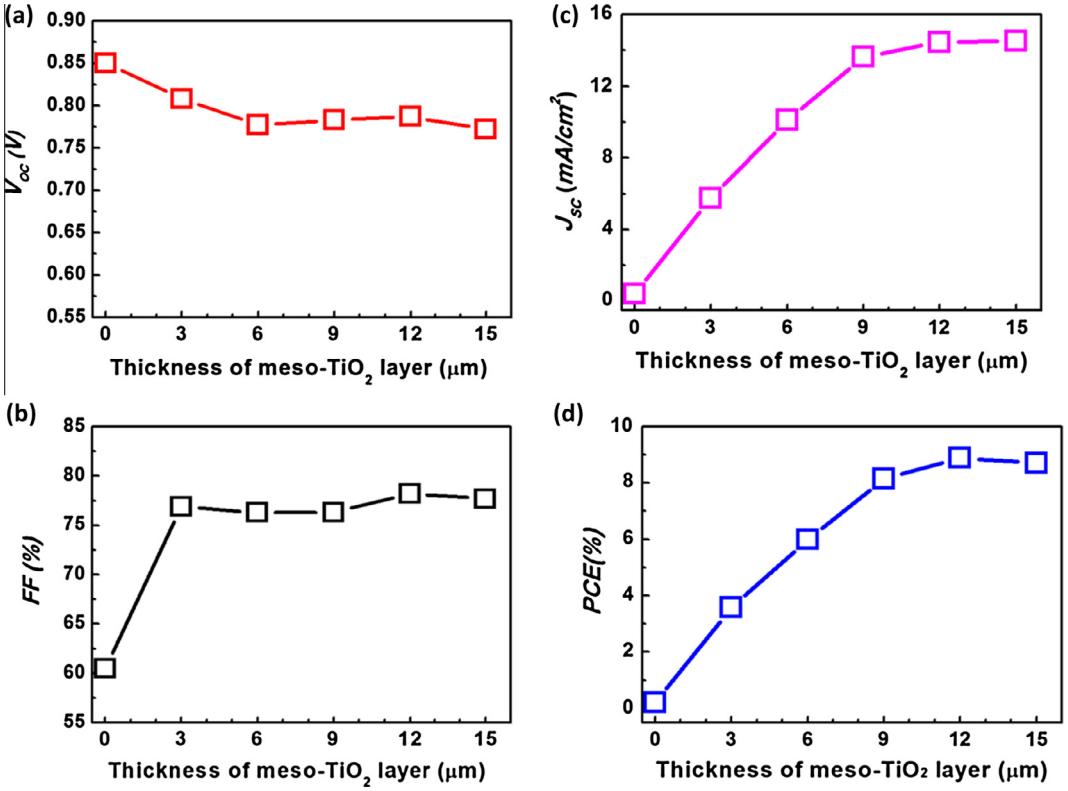

Fig. 8. (a) The correlation between open circuit voltage (V_{OC}) and the thickness of meso-TiO_2 NPs, (b) the correlation between short circuit current density (J_{SC}) and the thickness of meso-TiO_2 NPs, (c) the correlation between fill factor (*FF*) and the thickness of meso-TiO_2 NPs, and (d) the correlation between power conversion efficiency (*PCE*) and the thickness of meso-TiO_2 NPs.

working electrode and further enhanced light absorption behavior. After optimizing the parameters of DSSCs, the overall performance of the meso-TiO_2 NPs/Bi-doped TiO_2 NFs devices was dominated by J_{SC} until a maximum efficiency was attained at 12 μm-thick meso-TiO_2 NPs, which J_{SC} = 14.45 mA/cm^2, V_{OC} = 0.787 V, FF = 0.782 and η = 8.89%, respectively.

4. Conclusion

In summary, Bi-doped TiO_2 NFs have been synthesized successfully. From UV–vis reflection spectra, Bi doping can extend the absorption spectra of TiO_2 from UV band into visible light band. Then, we adopt Bi-doped TiO_2 NFs to further study in the application of DSSCs. The V_{OC} is significantly enhanced from ~0.6 V to more than 0.8 V by replacing pristine TiO_2 NFs with Bi-doped TiO_2 NFs. The incorporated Bi-doped TiO_2 NFs layer can increase the light scattering and the Fermi energy of TiO_2 electrode, and reduce the possibility for electron–hole recombination. After optimizing the thickness of TiO_2 electrodes, we adopt 3 μm Bi-doped TiO_2 NFs as the light scattering layer and 12 μm meso-TiO_2 NPs as the working electrode to assemble the DSSCs. The overall performance of the optimized DSSCs exhibits high open circuit voltage of 0.787 V and high power conversion efficiency of 8.89%.

Acknowledgements

Financial support obtained from the Ministry of Science and Technology of Taiwan (MOST 103-2221-E-182-008-MY2, MOST 104-3113-E-002-010, MOST 104-2632-E-182-001 and MOST 104-2923-M-002-009) and the Chang Gung University Research Project is highly appreciated. We thank Prof. Wei-Fang Su of the National Taiwan University and Dr. Ming-Tao Lee's group (BL-13A1) of the National Synchrotron Radiation Research Centre for useful discussion and suggestions.

Appendix A. Supplementary material

Supplementary data associated with this article can be found, in the online version, at http://dx.doi.org/10.1016/j.solener.2016.05.021.

References

Chen, C.-Y., Wang, M., Li, J.-Y., Pootrakulchote, N., Alibabaei, L., Ngoc-le, C.-H., Decoppet, J.-D., Tsai, J.-H., Grätzel, C., Wu, C.-G., Zakeeruddin, S.M., Grätzel, M., 2009. Highly efficient light-harvesting ruthenium sensitizer for thin-film dye-sensitized solar cells. ACS Nano 3, 3103–3109.

Chiappara, C., Figá, V., Marco, G.D., Calogero, G., Citro, I., Scuto, A., Lombardo, S., Pignataro, B., Principato, F., 2016. Investigation of recovery mechanisms in dye sensitized solar cells. Sol. Energy 127, 56–66.

Chou, C.-S., Guo, M.-G., Liu, K.-H., Chen, Y.-S., 2012. Preparation of TiO_2 particles and their applications in the light scattering layer of a dye-sensitized solar cell. Appl. Energy 92, 224–233.

Ding, J., Li, Y., Hu, H., Bai, L., Zhang, S., Yuan, N., 2013. The influence of anatase-rutile mixed phase and ZnO blocking layer on dye-sensitized solar cells based on TiO_2 nanofiber photoanodes. Nanoscale Res. Lett. 8, 9-9.

Ghanbari Niaki, A.H., Bakhshayesh, A.M., Mohammadi, M.R., 2014. Double-layer dye-sensitized solar cells based on Zn-doped TiO_2 transparent and light scattering layers: Improving electron injection and light scattering effect. Sol. Energy 103, 210–222.

Hore, S., Vetter, C., Kern, R., Smit, H., Hinsch, A., 2006. Influence of scattering layers on efficiency of dye-sensitized solar cells. Sol. Energy Mater. Sol. Cells 90, 1176–1188.

Horváth, E., Kukovecz, Á., Kónya, Z., Kiricsi, I., 2007. Hydrothermal conversion of self-assembled titanate nanotubes into nanowires in a revolving autoclave. Chem. Mater. 19, 927–931.

Konstantinou, I.K., Albanis, T.A., 2004. TiO_2-assisted photocatalytic degradation of azo dyes in aqueous solution: kinetic and mechanistic investigations. Appl. Catal. B 49, 1–14.

Kudo, A., Miseki, Y., 2009. Heterogeneous photocatalyst materials for water splitting. Chem. Soc. Rev. 38, 253–278.

Kudo, A., Kato, H., Tsuji, I., 2004. Strategies for the development of visible-light-driven photocatalysts for water splitting. Chem. Lett. 33, 1534–1539.
Li, S.S., Chang, C.P., Lin, C.C., Lin, Y.Y., Chang, C.H., Yang, J.R., Chu, M.W., Chen, C.W., 2011. Interplay of three-dimensional morphologies and photocarrier dynamics of polymer/TiO_2 bulk heterojunction solar cells. J. Am. Chem. Soc. 133, 11614–11620.
Lin, Y.-Y., Chu, T.-H., Li, S.-S., Chuang, C.-H., Chang, C.-H., Su, W.-F., Chang, C.-P., Chu, M.-W., Chen, C.-W., 2009. Interfacial nanostructuring on the performance of polymer/TiO_2 nanorod bulk heterojunction solar cells. J. Am. Chem. Soc. 131, 3644–3649.
Lü, X., Mou, X., Wu, J., Zhang, D., Zhang, L., Huang, F., Xu, F., Huang, S., 2010. Improved-performance dye-sensitized solar cells using Nb-doped TiO_2 electrodes: efficient electron injection and transfer. Adv. Funct. Mater. 20, 509–515.
Moghaddam, H.A., Mohammadi, M.R., Reyhani, S.M.S., 2016. Improved photon to current conversion in nanostructured TiO_2 dye-sensitized solar cells by incorporating cubic $BaTiO_3$ particles deliting incident. Sol. Energy 132, 1–14.
Nikolay, T., Larina, L., Shevaleevskiy, O., Ahn, B.T., 2011. Electronic structure study of lightly Nb-doped TiO_2 electrode for dye-sensitized solar cells. Energy Environ. Sci. 4, 1480–1486.
Ong, W.J., Tan, L.L., Chai, S.P., Yong, S.T., Mohamed, A.R., 2014. Highly reactive 001 facets of TiO_2-based composites: synthesis, formation mechanism and characterization. Nanoscale 6, 1946–2008.
O'Regan, B., Gratzel, M., 1991. A low-cost, high-efficiency solar cell based on dye-sensitized colloidal TiO_2 films. Nature 353, 737–740.
Park, S.-K., Han, Y.-S., 2014. Efficient dye-sensitized solar cells with surface-modified photoelectrodes. Sol. Energy 110, 260–267.
Rho, W.-Y., Chun, M.-H., Kim, H.-S., Hahn, Y.-B., Suh, J.S., Jun, B.-H., 2014. Improved energy conversion efficiency of dye-sensitized solar cells fabricated using open-ended TiO_2 nanotube arrays with scattering layer. Bull. Korean Chem. Soc. 35, 1165–1168.
Sarkar, A., Shchukarev, A., Leino, A.R., Kordas, K., Mikkola, J.P., Petrov, P.O., Tuchina, E.S., Popov, A.P., Darvin, M.E., Meinke, M.C., Lademann, J., Tuchin, V.V., 2012. Photocatalytic activity of TiO_2 nanoparticles: effect of thermal annealing under various gaseous atmospheres. Nanotechnology 23, 475711.
Wu, M.-C., Tóth, G., Sápi, A., Leino, A.-R., Kónya, Z., Kukovecz, Á., Su, W.-F., Kordás, K., 2012. Synthesis and photocatalytic performance of titanium dioxide nanofibers and the fabrication of flexible composite films from nanofibers. J. Nanosci. Nanotechnol. 12, 1421–1424.
Wu, M.-C., Chih, J.-S., Huang, W.-K., 2014. Bismuth doping effect on TiO_2 nanofibres for morphological change and photocatalytic performance. CrystEngComm 16, 10692–10699.
Xu, J., Li, K., Shi, W., Li, R., Peng, T., 2014. Rice-like brookite titania as an efficient scattering layer for nanosized anatase titania film-based dye-sensitized solar cells. J. Power Sources 260, 233–242.
Yella, A., Lee, H.-W., Tsao, H.N., Yi, C., Chandiran, A.K., Nazeeruddin, M.K., Diau, E.W.-G., Yeh, C.-Y., Zakeeruddin, S.M., Grätzel, M., 2011. Porphyrin-sensitized solar cells with cobalt (II/III) – based redox electrolyte exceed 12 percent efficiency. Science 334, 629–634.
Yu, J., Yang, Y., Fan, R., Zhang, H., Li, L., Wei, L., Shi, Y., Pan, K., Fu, H., 2013. Er^{3+} and Yb^{3+} co-doped $TiO_{2-x}Fx$ up-conversion luminescence powder as a light scattering layer with enhanced performance in dye sensitized solar cells. J. Power Sources 243, 436–443.
Zhang, Z., Hossain, M.F., Takahashi, T., 2010. Photoelectrochemical water splitting on highly smooth and ordered TiO_2 nanotube arrays for hydrogen generation. Int. J. Hydrogen Energy 35, 8528–8535.